Hindawi Publishing Corporation
Mathematical Problems in Engineering
Volume 2014, Article ID 752721, 17 pages
http://dx.doi.org/10.1155/2014/752721

Research Article

Influences of RVG Positions on the Periodic Flow Profiles

Withada Jedsadaratanachai

Department of Mechanical Engineering, Faculty of Engineering, King Mongkut's Institute of Technology Ladkrabang, Bangkok 10520, Thailand

Correspondence should be addressed to Withada Jedsadaratanachai; kjwithad@kmitl.ac.th

Received 9 March 2014; Revised 2 May 2014; Accepted 5 May 2014; Published 26 June 2014

Academic Editor: Mohamed A. Seddeek

The effects on the positions of rib vortex generators (RVGs) for periodic laminar flow behavior are presented numerically in three-dimensional. The RVGs with constant blockage ratio (b/H, BR = 0.15), the pitch ratio (P/H, PR = 1), and flow attack angle ($\alpha = 30^{\circ}$) are inserted in isothermal walls of the square channel. The SIMPLE algorithm and the finite volume method (FVM) are applied for the computational domain. The influences of different gap ratios (g/H = 0–0.35) for Reynolds number based on the hydraulic diameter (D_h), Re = 100–1200, are investigated. It is found that the flow profiles can be divided into two parts; the first, similar in flow configuration, but different in u/u_0 values, is called "periodic flow" and the second, similar in both flow configuration and u/u_0 values, is called "fully developed periodic flow." The results reveal that the periodic flow profiles appear around 2nd-3rd modules while the fully developed flow profiles occur around 6th–9th modules. In addition, the periodic flow profiles and fully developed periodic flow profiles become faster in case of the lowest continuous flow area (g/H = 0.20, 0.25, and 0.30) and the regimes close to the RVG.

1. Introduction

Due to the relationship between flow configuration and heat transfer, the study for enhancing heat transfer in heat exchanger system leads to the investigation on flow configuration. The use of vortex generators or turbulator, such as rib, baffle, and winglet, is a main aim to change the flow field and also to create the flow separation, secondary flow, and impinging jet flow for heat transfer augmentation. The investigations on flow structure and heat transfer are separated into two methods, experimental and numerical. Owing to the limitation of experimental measurement, high cost materials and more time for study, therefore, the numerical method is advantages for study flow configurations and heat transfer characteristics. However, the investigation with the numerical method needs the high accuracy of mathematical model and condition for calculation.

As the requirements above, the periodic concept on flow configuration is extensively applied in the numerical model to approximate the large heat transfer system that leads to the low cost and saves more time for the simulation. Many investigations use periodic concept to study the flow configuration, heat transfer enhancement, and thermal performance. For example, Sripattanapipat and Promvonge [1] numerically studied the laminar periodic flow and thermal behaviors in a two-dimensional channel fitted with staggered diamond-shaped baffles. They found that the diamond baffle with half apex angle of 5–10° slightly performs better flow than flat baffle. Promvonge et al. [2] also examined numerically with periodic concept on the laminar heat transfer in a square channel with 45° angled baffle placed on one wall. They reported that a single streamwise vortex flow appears and also induces impingement jets on the wall of the interbaffle cavity and the BTE sidewall. Moreover, Promvonge et al. [3, 4] also applied the numerical manner to investigate the laminar flow structure and thermal behaviors in a square channel with 30° or 45° inline baffles on two opposite walls using periodic concept on both flow behavior and heat transfer characteristics. Two streamwise counter-rotating vortex flows were created along the channel and vortex-induced-impingement jets appeared on the upper and lower sides of the tested channel and baffle leading end side walls while the maximum thermal enhancement factors of about 2.6 at BR = 0.20, PR = 1, and Re = 1000 and of around 4.0 at BR = 0.15, PR = 2, and Re = 2000 for using the 45° and 30° baffles were reported, respectively. The numerical investigations for

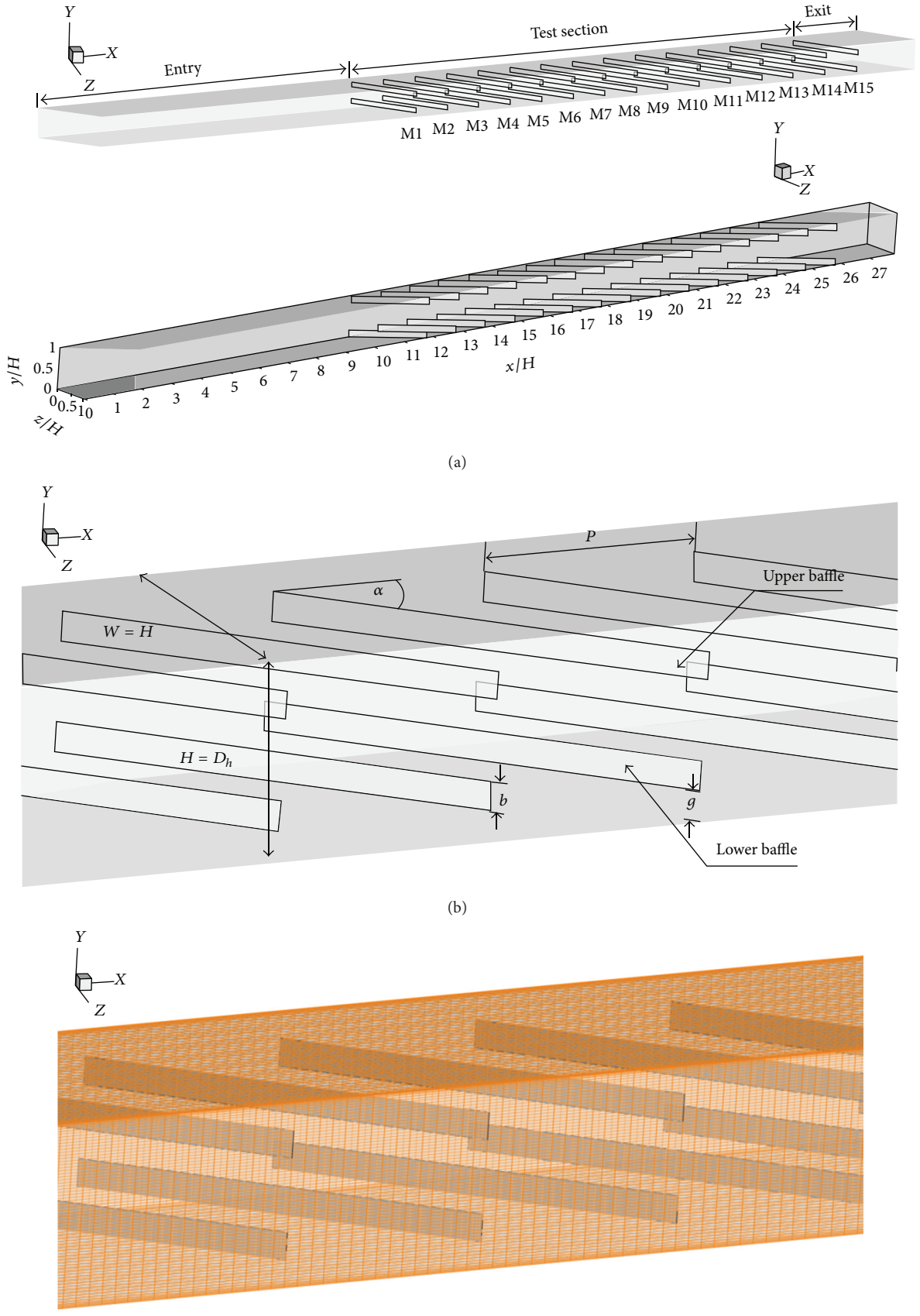

Figure 1: (a) Square channel with RVG, (b) details of square channel with RVG, (c) computational domain.

Table 1: The literature reviews for numerical investigation with using periodic concept.

Authors	Studied cases	Nu/Nu_0	f/f_0	TEF
Jedsadaratanachai et al. [5]	30° inclined baffle Inline, two opposite walls, square channel BR = 0.2 PR = 0.5–2.5 Re = 100–2000	1.00–9.20	1.00–21.50	3.78
Kwankaomeng and Promvonge [9]	30° inclined baffle One side, square channel BR = 0.1–0.5 PR = 1.0–2.0 Re = 100–1000	1.00–9.23	1.09–45.31	3.10
Promvonge et al. [3]	30° inclined baffle Inline, two opposite walls, square channel BR = 0.1–0.3 PR = 1.0–2.0 Re = 100–2000	1.20–11.00	2.00–54.00	4.00
Promvonge and Kwankaomeng, [10]	45° V-baffle Staggered, two opposite walls, AR = 2 channel BR = 0.05–0.3 PR = 1.0 Re = 100–1200	1.00–11.00	2.00–90.00	2.75
Promvonge et al. [2]	45° inclined baffle Inline-staggered, two opposite walls, square channel BR = 0.05–0.3 PR = 1.0 Re = 100–1000	1.50–8.50	2.00–70.00	2.60
Promvonge et al. [4]	45° V-baffle Inline downstream, two opposite walls, square channel BR = 0.1–0.3 PR = 1.0–2.0 Re = 100–2000	1.00–21.00	1.10–225.00	3.80
Boonloi [11]	20° V-baffle Inline downstream-upstream, two opposite walls, square channel BR = 0.1–0.3 PR = 1.0 Re = 100–2000	1.00–13.00	1.00–52.00	4.20
Boonloi and Jedsadaratanachai [12]	30° V-baffle Downstream, one side, square channel BR = 0.1–0.5 PR = 1.0–2.0 Re = 100–1200	1.00–14.49	2.18–313.24	2.44
Jedsadaratanachai and Boonloi [13]	45° discrete-V-baffle Downstream, diagonally, square channel BR = 0.05–0.20 PR = 1.0–1.5 Re = 100–1200	1.40–8.10	2.50–36.00	2.50
Jedsadaratanachai and Boonloi [14]	Single twisted tape y/W = 1.0–6.0 Re = 100–2000	1.00–10.00	3.00–44.00	3.51

laminar forced convection with using periodic concept are summarized in Table 1.

Except from the use of periodic concept to study heat transfer and flow structure, the descriptions of behavior for the periodic flow structure and periodic heat transfer behavior were reported. Jedsadaratanachai et al. [5] studied laminar forced convection in a tube with turbulators and concluded that the flows in baffled tube show periodic flow at x/D = 2-3 and become a fully developed periodic flow profile at x/D = 6-7, depending on Re, BR, and transverse

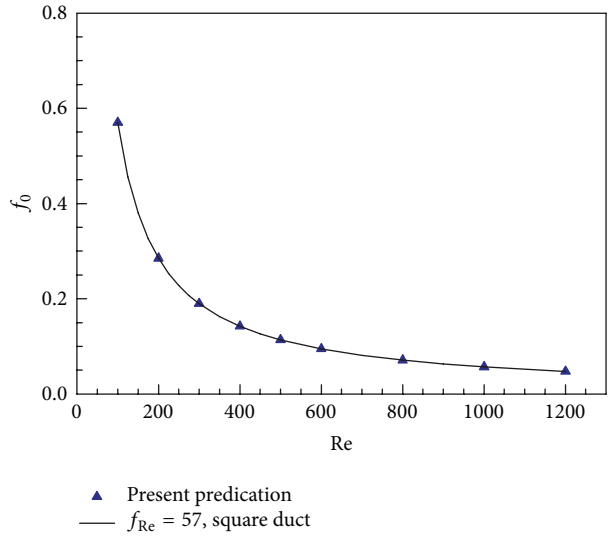

Figure 2: Validation of friction factor for smooth square channel.

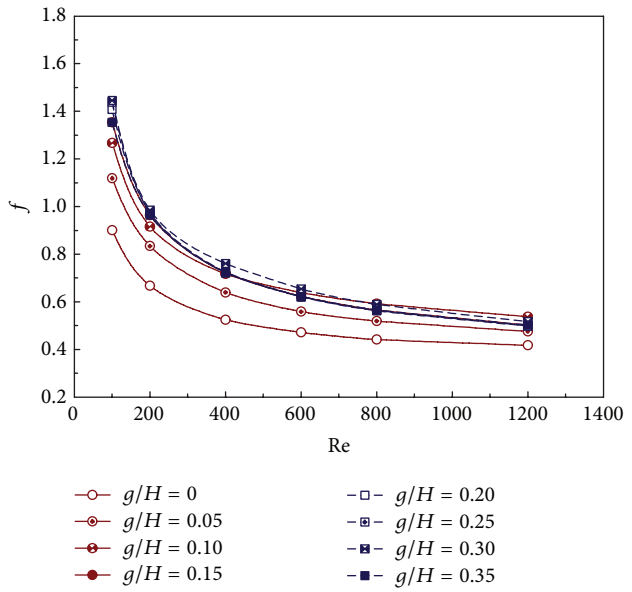

Figure 3: The variations of friction factor with Re at various g/H.

plane positions. They concluded that the rise of BR and close to the turbulators lead to faster of fully developed periodic profiles. Promvonge et al. [6] investigated flow configuration and heat transfer in square channel with V-baffle. They found that fully developed periodic flow and heat transfer profile for BR = 0.2 appeared around $x/D \approx 8$ downstream of the inlet. Jedsadaratanachai et al. [7] found that the decrease of PR result in a speedup of fully developed periodic flow configuration.

As the literature above, most investigations studied the effect of blockage ratio, pitch ratio, and Reynolds number on the developing periodic flow and heat transfer behavior. Therefore, the study of the influence on the position of the vortex generators for developing the periodic flow concept has rarely been reported. In this present work, the investigation on the effect of positioning on vortex generators for the periodic flow concept is presented numerically in three dimensional. The different gap ratios, g/H = 0–0.35, for 30° inclined rib vortex generators (RVGs) with constant BR = 0.15 and PR = 1.00 are studied.

2. Square Channel Geometry and Numerical Domain

All of the methodologies for numerical investigation are following [5–7]. Figures 1(a), 1(b), and 1(c) show a square channel with RVGs inserted, details of testing channel, and

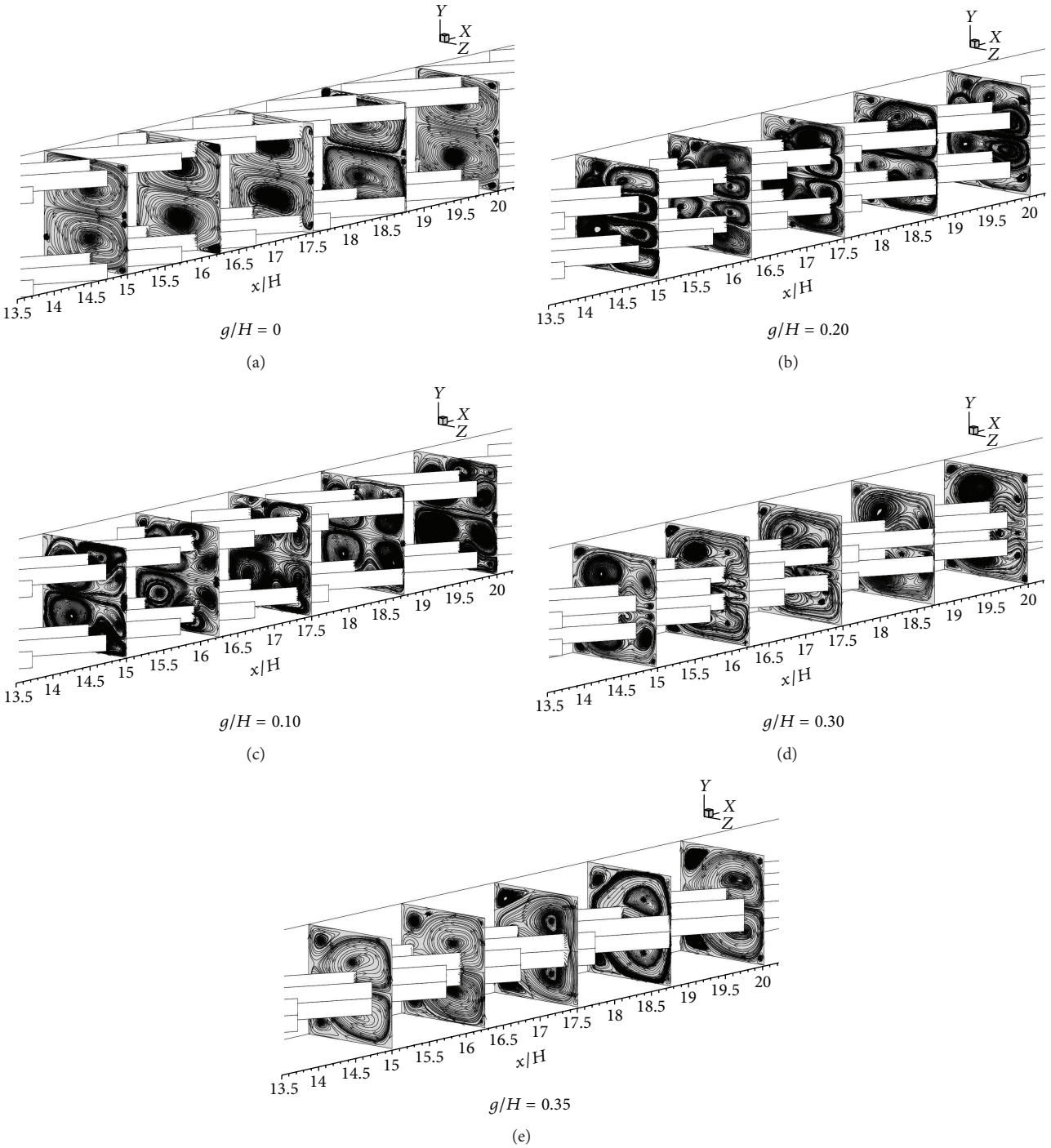

Figure 4: Streamlines in transverse planes at various g/H for Re = 800.

the computational domain, respectively. The 30° RVGs are arranged with inline arrangement and placed on both the upper and lower parts of the testing channel. In the tested channel, the air enters at an inlet temperature, T_{in}, and flows over RVGs where b is the RVG height, H is set to 0.05 m, which is the channel height and b/H is known as the blockage ratio, BR = 0.15. The longitudinal distance between the RVGs is set to P in which P/H is defined as the pitch ratio, PR = 1.0. The positions of RVG are varied by considering the distance between the upper and lower walls of the square channel to the RVG, g, and g/H is identified as the gap ratio. To investigate an interaction influence of the RVG positions with an attack angle, $\alpha = 30^{\circ}$ is varied in a range of $g/H = 0$–0.35 in the present study. The 125,500 hexahedral cells of grid system have been applied to present computational domain causing no advantage to increase the number of grid cells.

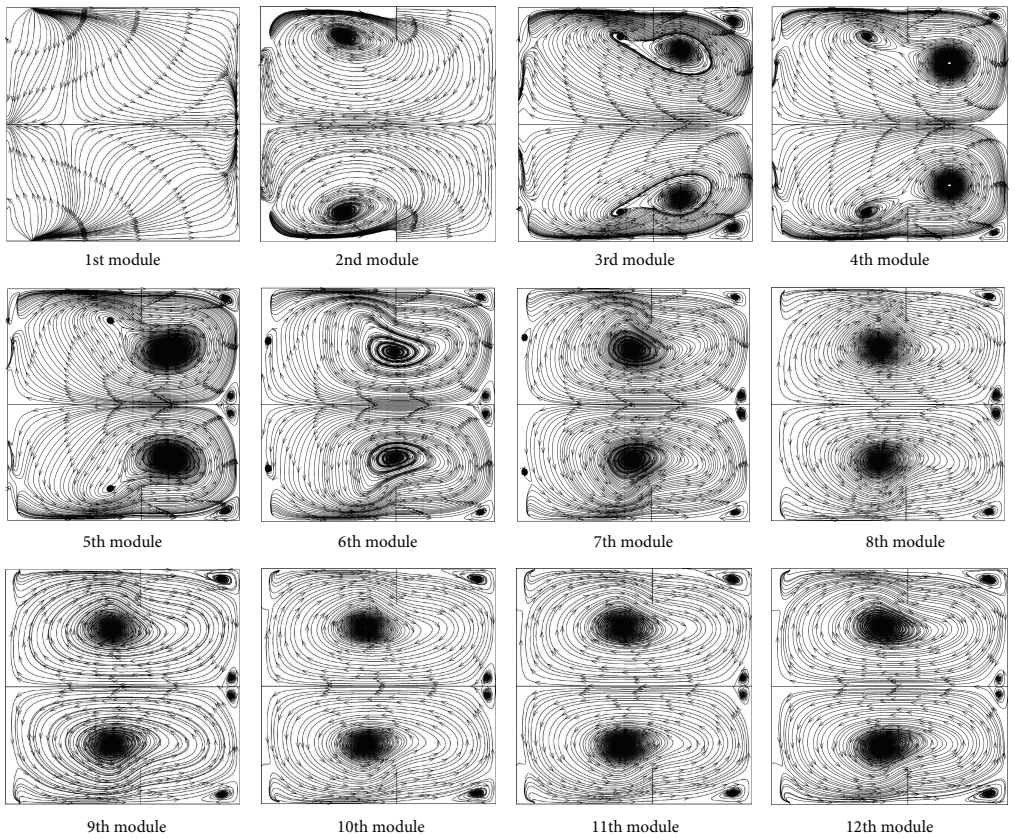

Figure 5: Streamlines in transverse planes for $g/H = 0$ at Re = 800.

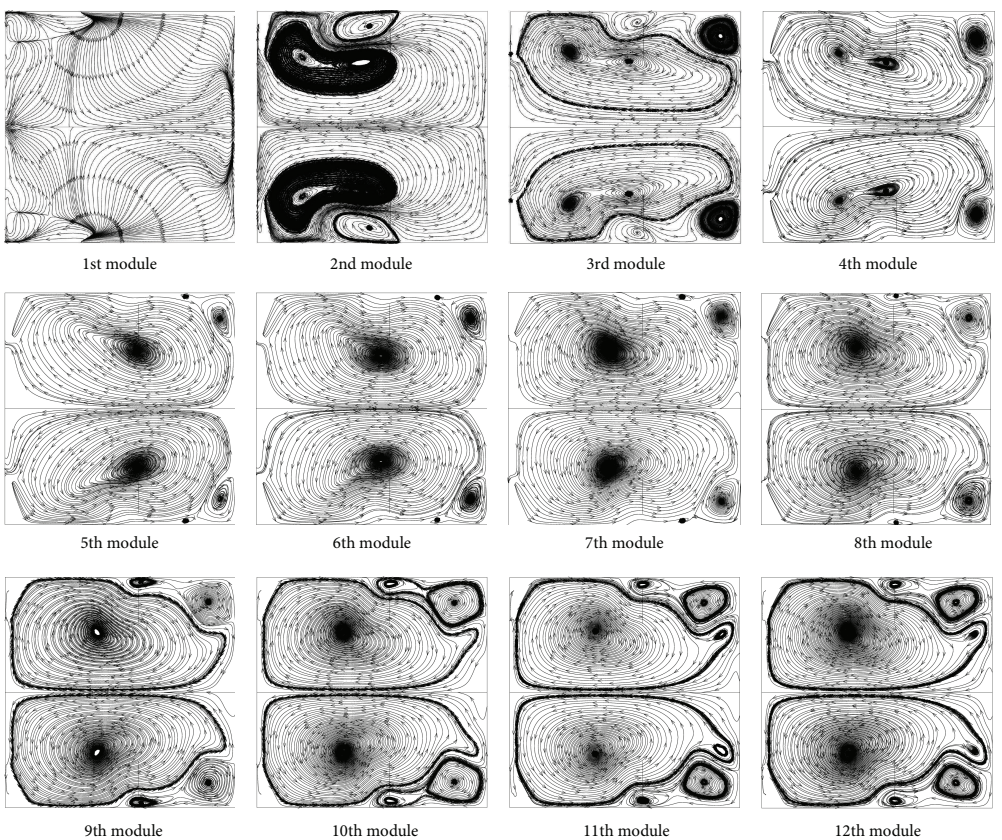

Figure 6: Streamlines in transverse planes for $g/H = 0.05$ at Re = 800.

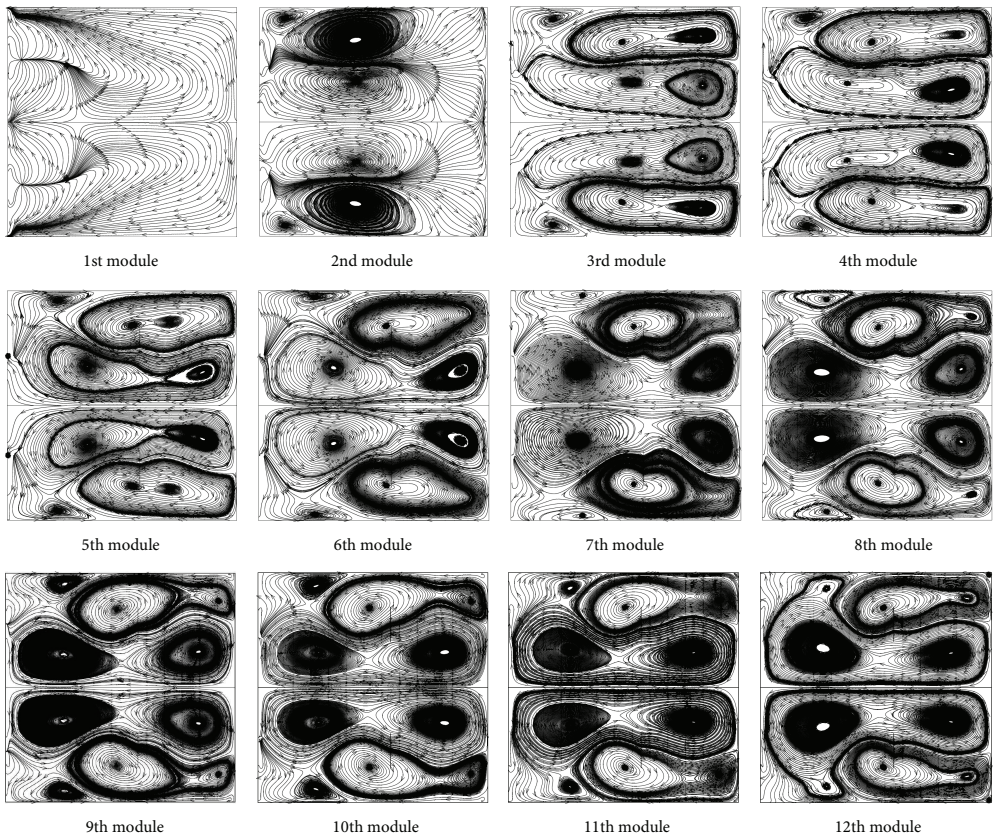

Figure 7: Streamlines in transverse planes for $g/H = 0.15$ at Re = 800.

The variation of the friction factor is less than ±0.2% when increasing numbers of grid cell.

3. Mathematical Foundation and Boundary Condition

The mathematical foundations for the present work are referred from [5–7]. The numerical model for fluid flow in a square channel was developed under the following assumptions:

(i) steady three-dimensional fluid flow,

(ii) the flow is laminar and incompressible,

(iii) constant air properties,

(iv) body forces and viscous dissipation are ignored.

Based on the above assumptions, the relevant equation is the Navier-Stokes equation. The equations in the tensor notation form are as follows.

Continuity equation:

$$\frac{\partial}{\partial x_i}\left(\rho u_i\right) = 0. \tag{1}$$

Momentum equation:

$$\frac{\partial\left(\rho u_i u_j\right)}{\partial x_j} = -\frac{\partial p}{\partial x_i} + \frac{\partial}{\partial x_j}\left[\mu\left(\frac{\partial u_i}{\partial x_j} + \frac{\partial u_j}{\partial x_i}\right)\right]. \tag{2}$$

The governing equations were discretized by the power law scheme, decoupling with the SIMPLE algorithm, and solved using a finite volume approach [8]. The solutions were measured to be converged when the normalized residual values were less than 10^{-6} for all variables.

The calculations of the two parameters including the Reynolds number, Re, and friction factor, f, are described by (3) and (4), respectively. Consider

$$\mathrm{Re} = \frac{\rho \bar{u} D}{\mu}. \tag{3}$$

The friction factor, f, is computed by pressure drop, Δp across the length of the module, and P as follows:

$$f = \frac{\left(\Delta p/P\right) D}{(1/2)\,\rho \bar{u}^2}. \tag{4}$$

3.1. Boundary Conditions. The boundary conditions are following [5–7]. For tested square channel, a uniform air velocity is introduced at the inlet while a pressure outlet condition is applied at the exit. The physical properties of the air have been assumed to constant at mean bulk temperature. Impermeable boundary and no-slip wall conditions have been implemented over the square channel walls as well as the RVG.

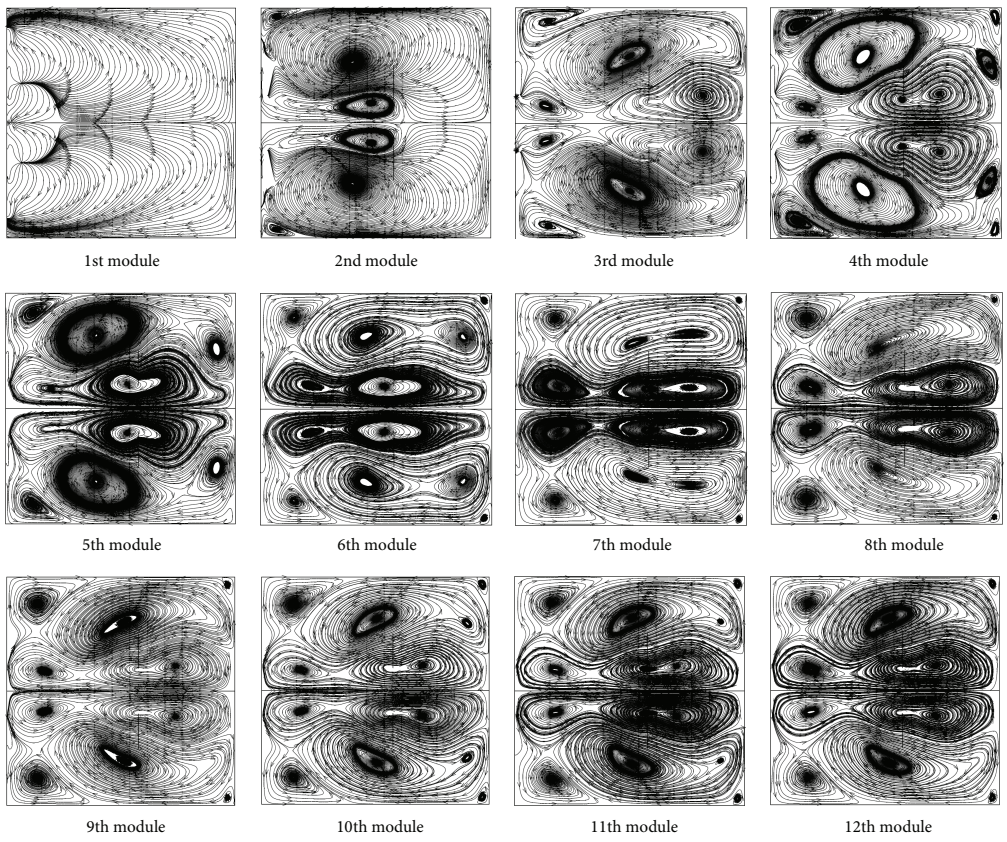

Figure 8: Streamlines in transverse planes for $g/H = 0.25$ at Re = 800.

4. Results and Discussion

4.1. Accuracy Validation. The validation of the smooth square channel with no RVG for this current investigation is tested by comparing the present prediction with the correlation of the friction factor values at various Reynolds numbers as shown in Figure 2. The result shows around ±0.5% deviation of the friction factor for all Reynolds numbers. The good agreement between the results from present prediction and correlation indicates that the numerical model is reliable to predict the flow characteristics in the square channel.

4.2. Flow Configuration. Figure 3 shows the variations of the friction factor with Reynolds number at various g/H values. As seen, the friction factor tends to decrease with the rise of Reynolds number for all cases. The $g/H = 0$ performs the lowest values of friction factor for all the Reynolds number. In range $0.20 \leq g/H \leq 0.35$, the friction factor nearly provides values and varies between 0.5 and 1.45. This means that the $g/H > 0.1$ results in the rise of friction factor.

The flow profiles for RVG at various g/H values are presented in Figure 4. It is necessary to understand the general flow structure and behavior in the square channel with placed RVG. The flow configuration for a module (five different positions, module/4) is presented in terms of streamlines in transverse planes at various g/H values for Re = 800 at the fully developed periodic flow regime, $x/H > 10$. It is found that the RVG produces two main counter-rotating vortex flows on the upper and lower parts due to the symmetry of the testing channel clearly seen as cases $g/H = 0$ and 0.35 for the RVGs placing on the lower walls and in the middle of the square channel, respectively, but reverse in the flow rotation. In the range $0 < g/H < 0.35$, the numbers of the small vortex flow perform higher, especially, $g/H = 0.10$ and 0.20. The decreasing continuous flow areas are the reason of the rise up of the numbers for the small vortex flow. In addition, the phenomenon of the flow structure at first plane ($x/H = 15$) is similar to the fifth plane ($x/H = 20$) in all cases. This means that the flow structures in the square channel with RVG perform periodic profiles or repeat themselves from one cell to another although the RVG positions are not similar.

4.3. Periodic Flow Descriptions. The periodic flow descriptions are presented in the forms of the streamlines in transverse planes at similar position of each module and the variations of u/u_0 with various positions. The twelve planes of the streamlines in transverse planes are plotted as Figures 5 to 9. As seen, the flow configuration can be divided into two zones, developing flow profile and the periodic flow profile. The developing flow profiles are found in the early regimes downstream from the inlet; the flow configuration has the main flow structure similar to other planes, but the core flow positions are found to be different. The periodic flow profiles, the flow behaviors, and the core flow positions appear to be similar when passing around the 5th module.

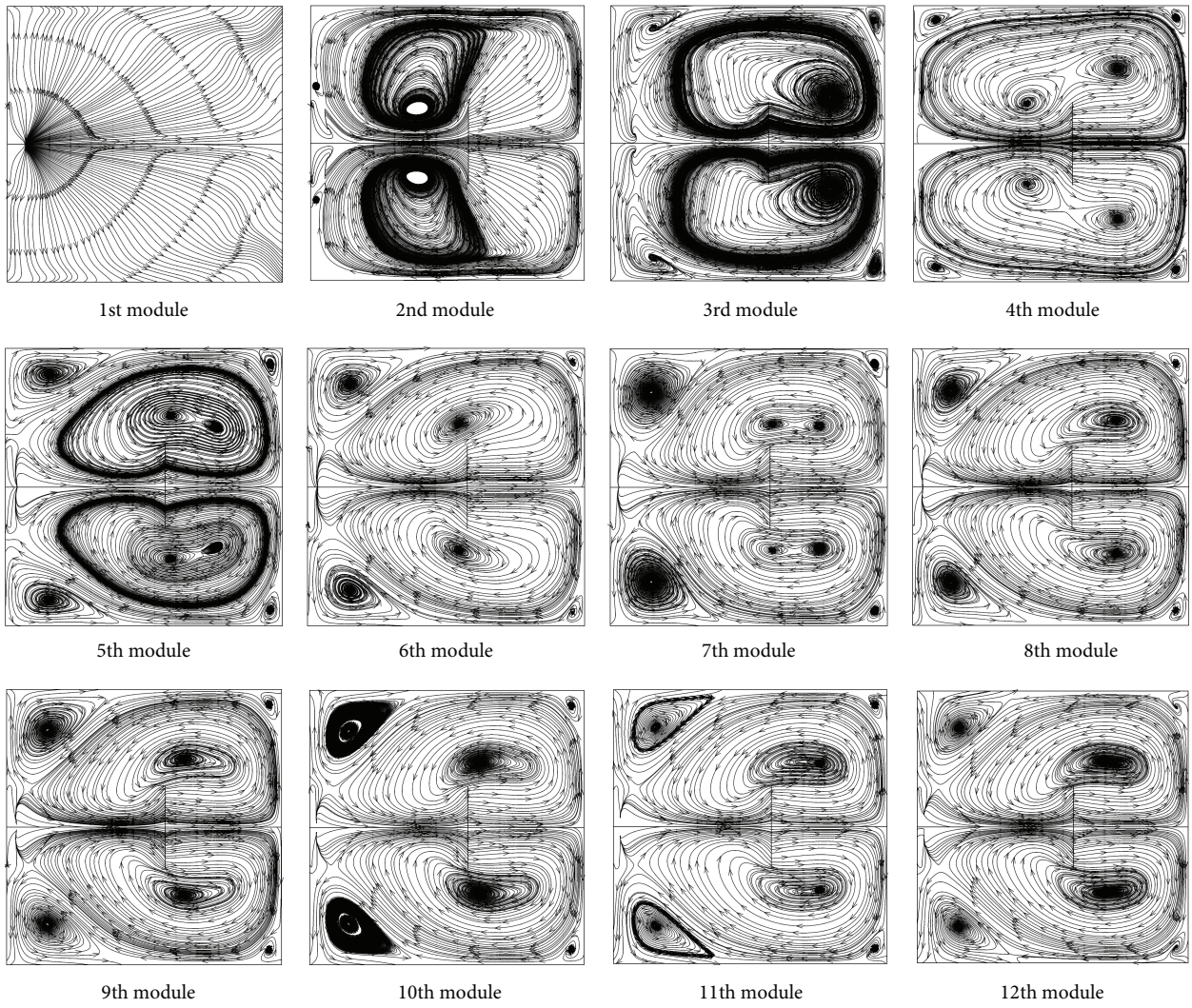

Figure 9: Streamlines in transverse planes for g/H= 0.35 at Re = 800.

For g/H = 0, the streamlines in transverse planes for twelve modules are presented in Figure 5 at Re = 800. As the figure, the two main counter-rotating vortex flows appear for all planes except for the first plane. In the 2nd–6th modules, developing flow profiles, the variations of the core flow positions are found. After the flows pass through the 6th module (7th–12th modules), periodic flow profiles, the flow configurations, and core flow positions seem to be similar.

The streamlines in transverse planes for g/H = 0.05 are shown in Figure 6. In general, the flow structures of this case seem to be likely as g/H = 0 and the small vortices appear at the upper and lower right corners of the tested square channel. The developing flow profiles appear around the 1st–8th modules and then the flows pass the 9th–12th modules; the periodic flow configuration is established.

The streamlines in transverse planes for g/H = 0.15 and 0.25 are presented as Figures 7 and 8, respectively, at Re = 800. The decrease in continuous-flow area result in the change of flow structure in the channel. The vortex flows with similar sizes appeared because of the decreasing continuous flow areas for both cases. The developing flow regimes perform shorter, but the periodic flow profiles become faster. The 1st–4th modules and 5th–15th modules are found to be developing flow profiles and periodic flow profiles, respectively, for g/H = 0.15 and 0.25. In addition, the decreasing flow areas result in the speed up of the periodic flow profiles.

The two main counter-rotating vortex flows that are similar as g/H = 0 with reversing rotation are found at g/H = 0.35 as presented in Figure 9. The periodic flow profiles occurred after the 8th module while the developing flow profiles are found at the 1st–7th modules.

In addition, the presentations on this part may be described roughly as flow configuration in the RVG tested channel but cannot identify for the equivalent value of the velocity on the x, y, and z directions, so the variations of velocity in terms of u/u_0 with different x/H, y/H, and z/H are presented in the next part.

4.4. The Variations of u/u_0. The variations of u/u_0 with x/H at various y/H and z/H values for g/H = 0, 0.10, 0.20, and 0.30 are presented as Figures 10, 11, 12, and 13, respectively, at Re =

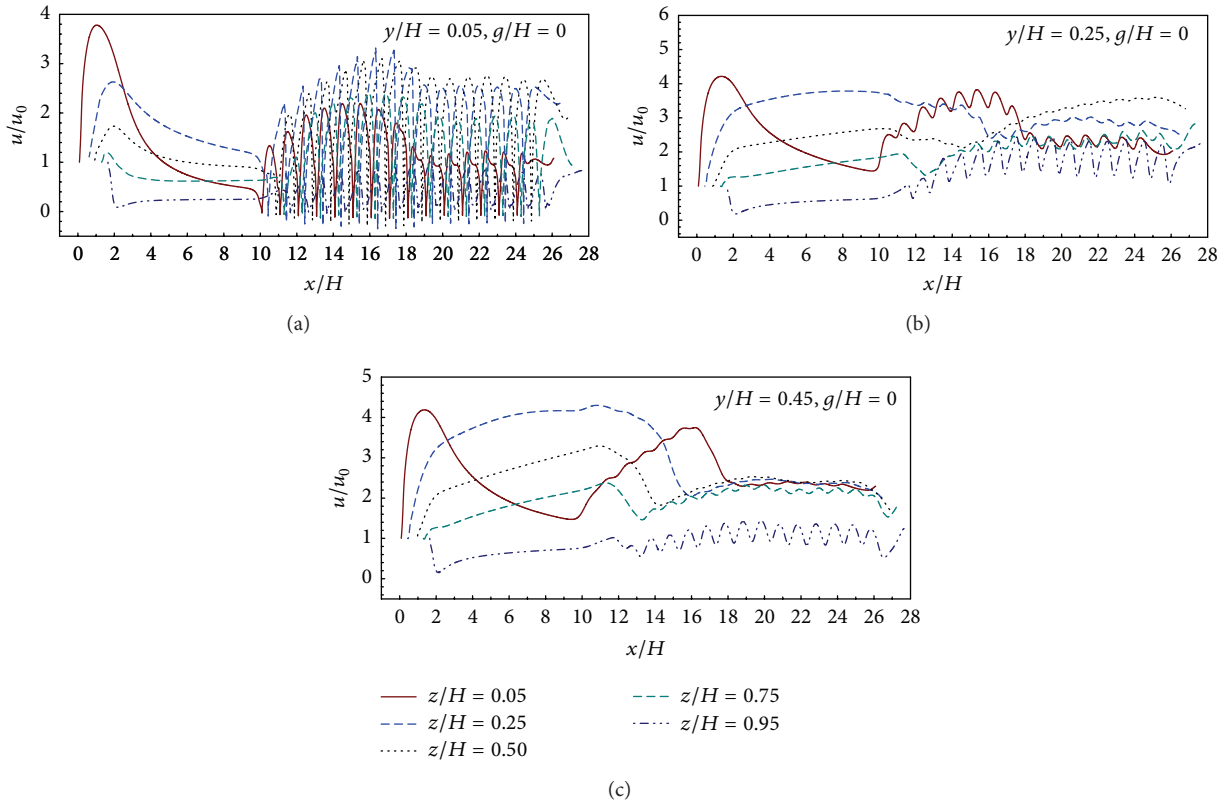

FIGURE 10: The variations of u/u_0 with x/H at various $y/H = 0.05$, 0.25, and 0.45 for $g/H = 0$ and Re = 800.

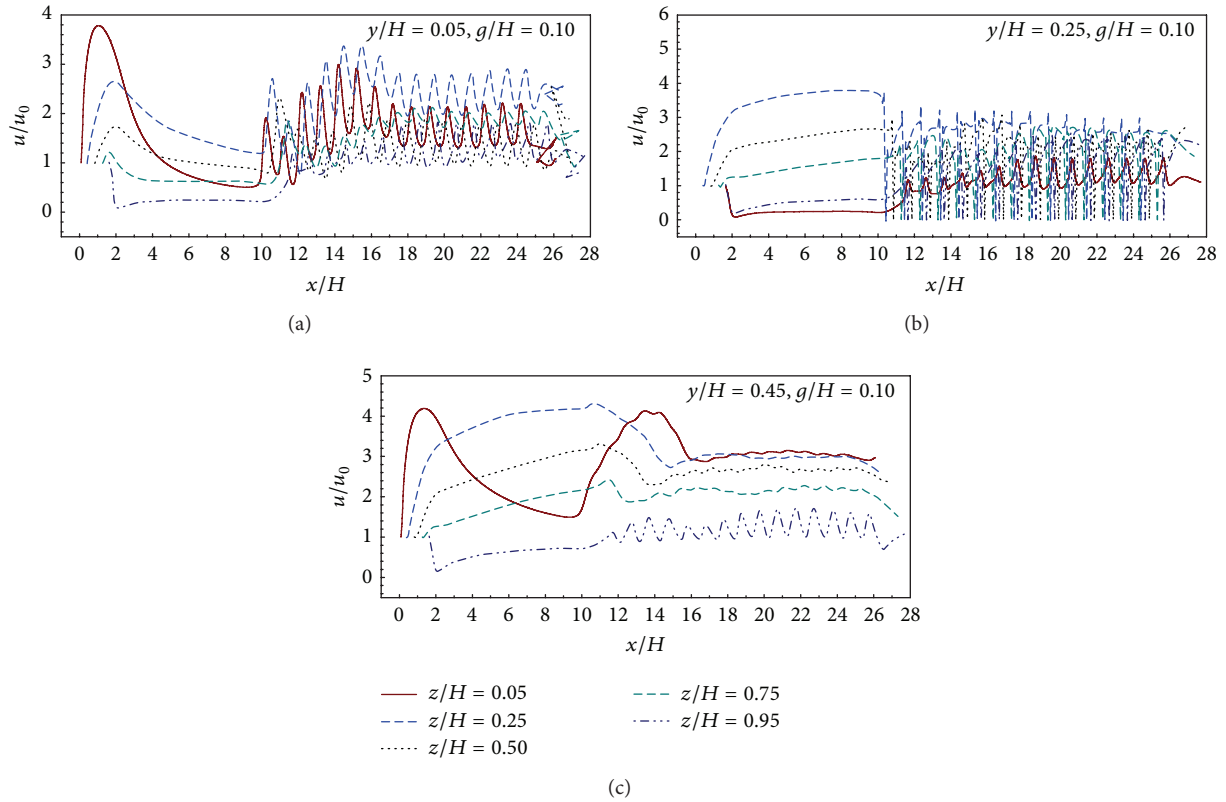

FIGURE 11: The variations of u/u_0 with x/H at various $y/H = 0.05$, 0.25, and 0.45 for $g/H = 0.10$ and Re = 800.

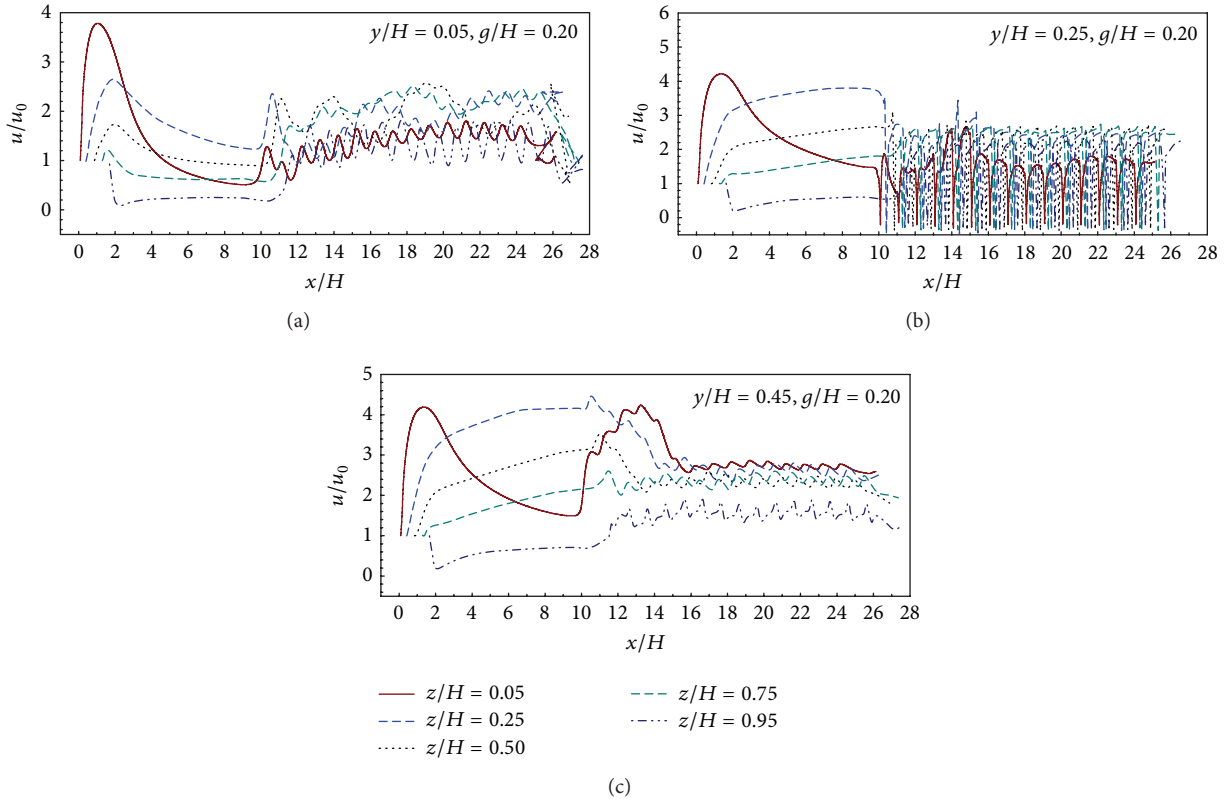

Figure 12: The variations of u/u_0 with x/H at various $y/H = 0.05$, 0.25, and 0.45 for $g/H = 0.20$ and Re = 800.

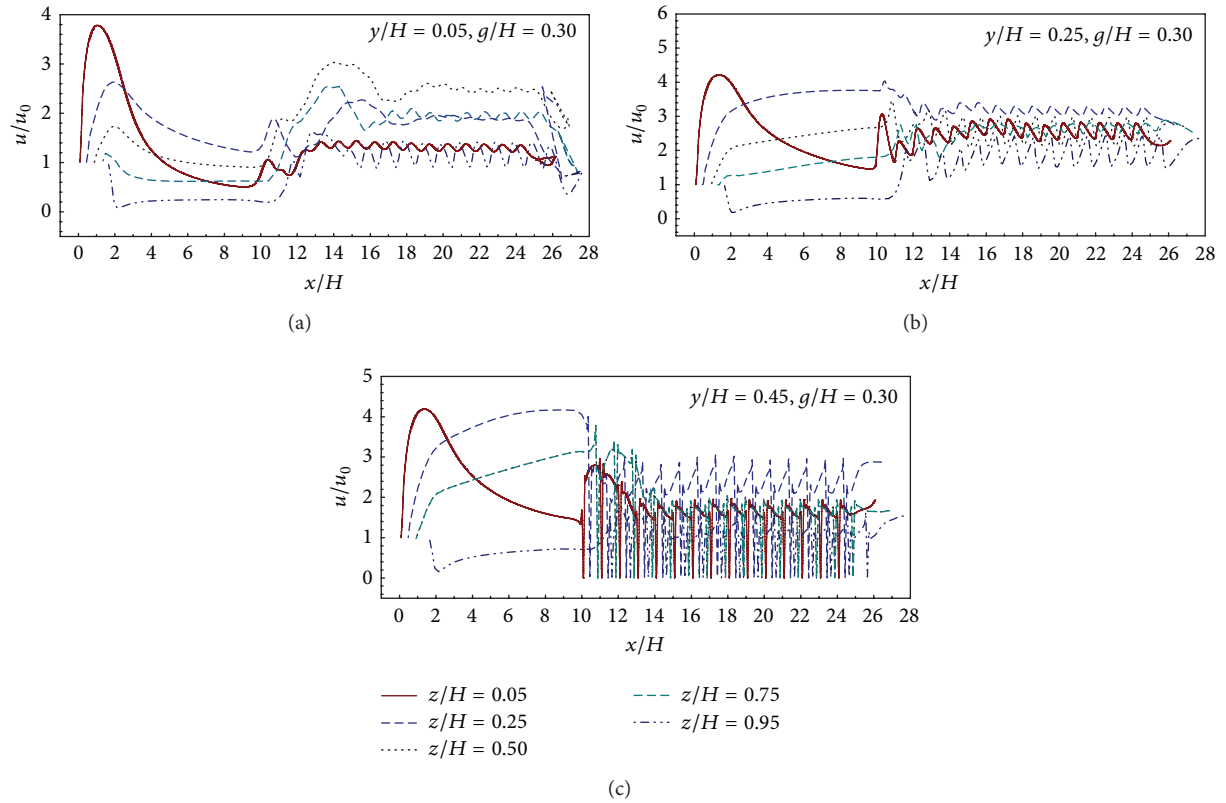

Figure 13: The variations of u/u_0 with x/H at various $y/H = 0.05$, 0.25, and 0.45 for $g/H = 0.30$ and Re = 800.

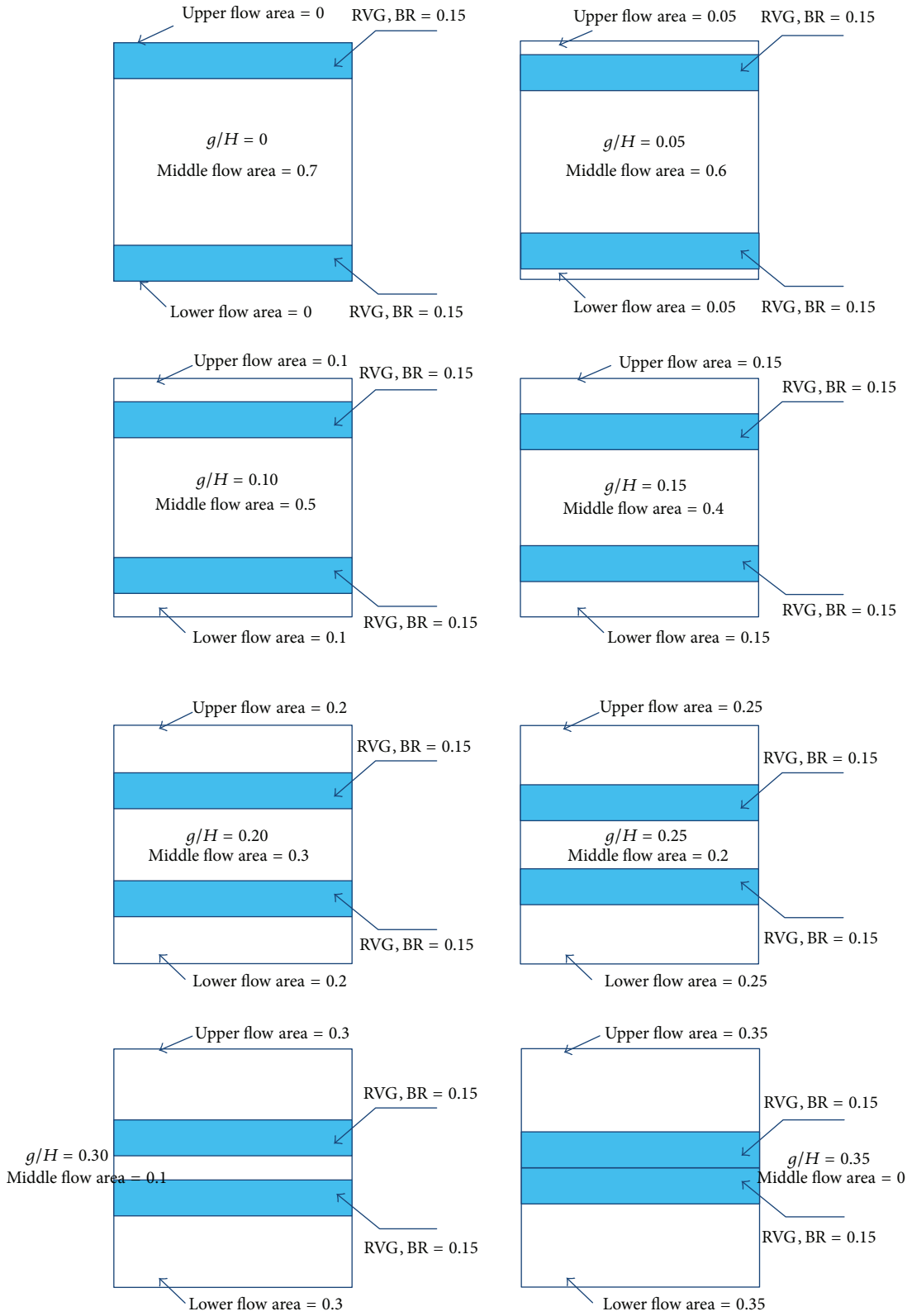

Figure 14: The flow area descriptions at various g/H.

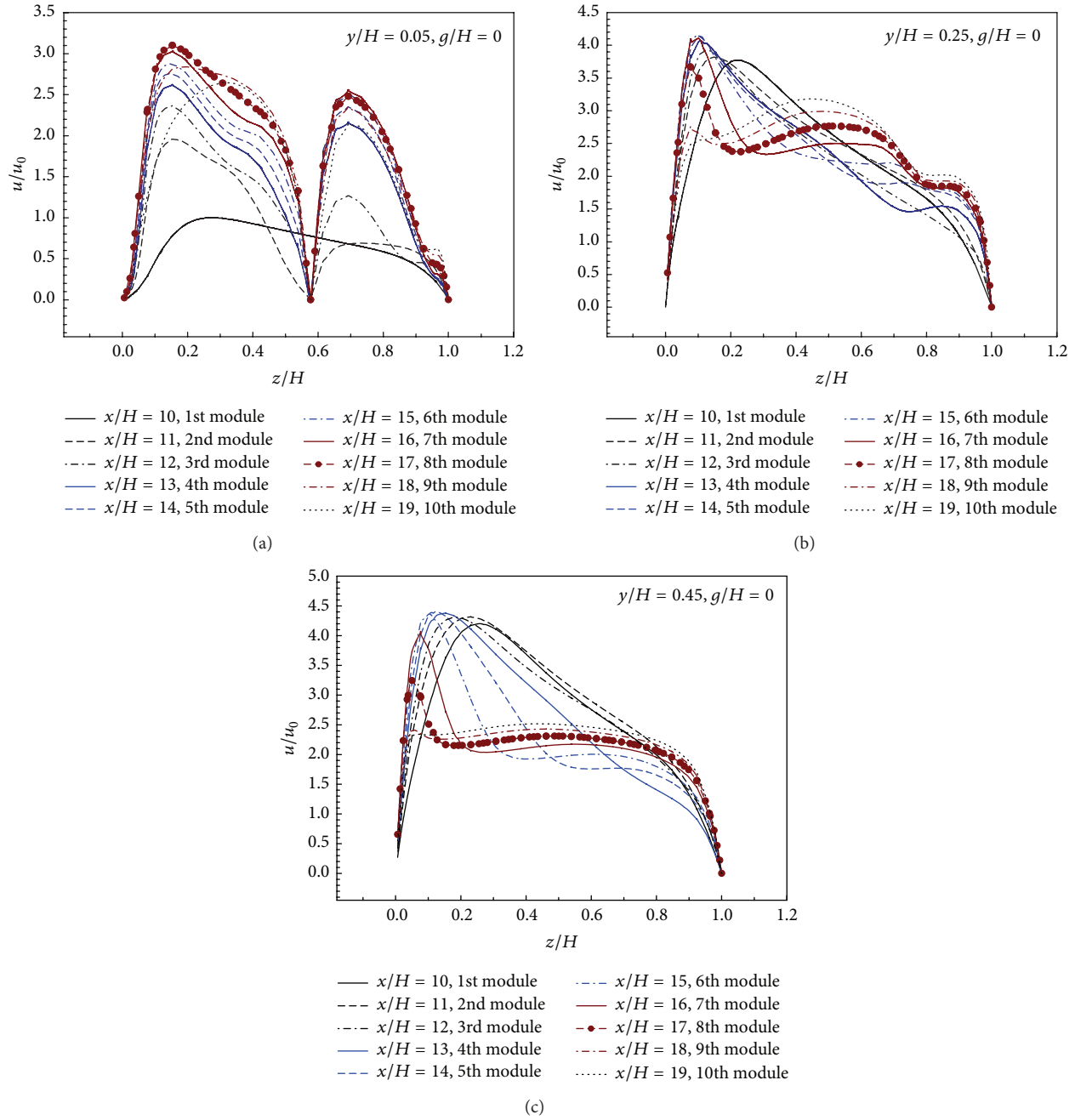

FIGURE 15: The variations of u/u_0 with z/H at various $y/H = 0.05$, 0.25, and 0.45 for $g/H = 0$ and Re = 800.

800. As the numerical results, the velocity profiles for all cases are divided into two groups. The similar velocity profiles but different from the values called "periodic flow profile" while the similarities in both structures and values of the velocity called "fully developed periodic flow profile". In general, the periodic flow profiles are found in the early regimes of the test section while the fully developed periodic profiles are appearing after flow passing around the 6th-8th module of the RVG.

The periodic flow profiles appear around the 2nd module (x/H = 11) and become the fully developed periodic flow profiles around the 8th–10th modules (x/H = 17–20) for all z/H values at $y/H = 0.05$. In ranges $y/H = 0.25$ and 0.45, the periodic flow profiles occur around the 2nd–5th modules and happen into the fully developed flow profiles around the 10th module only near sidewalls regime, $z/H = 0.05$ and 0.95.

The similar results as $g/H = 0$ of the development to the periodic and the fully developed periodic flow profiles are found in $g/H = 0.10$ that are plotted in Figure 11. The clarifications of the pattern for periodic flow profiles and the fully developed periodic flow profiles are seen when $y/H = 0.05$ and 0.25, especially, near the sidewall regimes, $z/H = 0.05$ and 0.95.

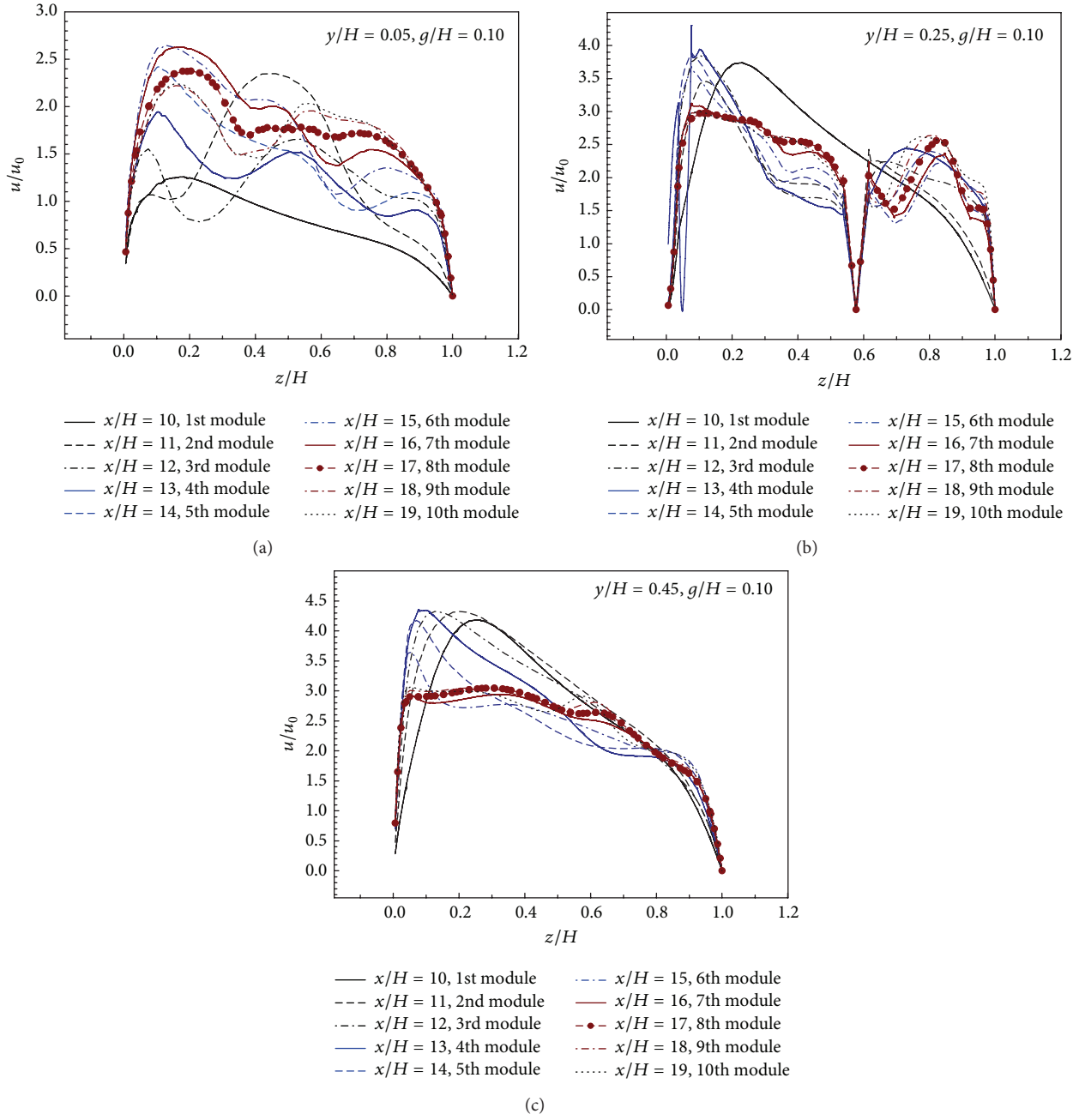

FIGURE 16: The variations of u/u_0 with z/H at various y/H = 0.05, 0.25, and 0.45 for g/H = 0.10 and Re = 800.

As seen in Figure 12, the y/H = 0.25 shows the flow configurations of the periodic flow profiles and the fully developed periodic flow profiles most clearly for g/H = 0.20 while y/H = 0.05 and 0.45, the periodic concepts, remain occurring on both sidewalls of the square channel only.

In Figure 13, g/H = 0.30, the periodic flow profiles and fully developed periodic flow profiles appeared for all of y/H values, especially, y/H = 0.45. This means that the reduction of the continuous-flow area is a key for appearing periodic profiles.

The RVG arrangements in y-z plane can be concluded as in Figure 14 and Table 2. The flow areas are divided into three groups: the upper flow area, the lower flow area, and the middle flow area. The increasing g/H value leads to the rise of upper and lower flow areas, but it decreases in the middle flow area. As the numerical results above, the periodic flow profiles perform fastest in case g/H = 0.15–0.25.

The variations of u/u_0 with z/H for g/H = 0, 0.10, 0.20, and 0.30 are shown in Figures 15, 16, 17, and 18, respectively, at Re = 800. In general, the velocity profiles in transverse z/H lines nearly appear to be a pattern of all g/H values. The fully developed periodic flow profiles are found around the 7th–9th modules relating to the velocity in x/H lines. It is noted that the $g/H > 0.05$; the periodic flow profiles did not appear

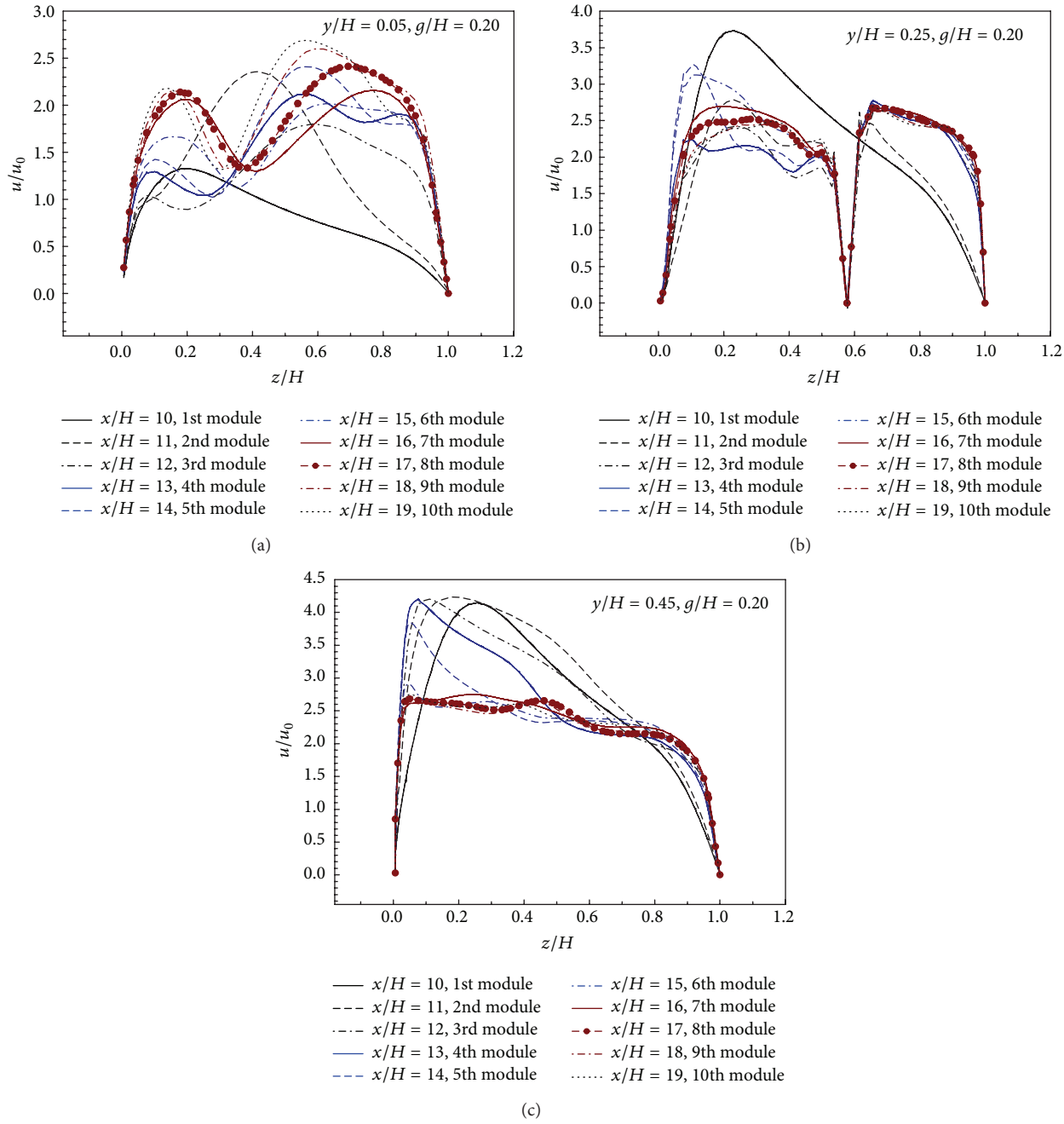

Figure 17: The variations of u/u_0 with z/H at various $y/H = 0.05$, 0.25, and 0.45 for $g/H = 0.20$ and Re = 800.

close to the upper and lower walls or on the gap between the walls and RVG of the channel ($y/H = 0.05$). In addition, with the variations of u/u_0 with y/H, the periodic flow profiles and fully developed periodic flow profiles are found similar to the results of the x/H lines for all cases.

5. Conclusion

The numerical investigations on the effects of RVG positions on the periodic flow concept are presented in three dimensional. The 30° RVG insert in the square channel with inline arrangement on both the upper and lower parts. The constants BR = 0.15 and PR = 1.0 with various $g/H = 0$–0.35 are used for the computational study. The numerical results can be summarized as follows.

(i) The friction factor tends to decrease with the rise of Reynolds number for all cases. In range $0 \leq g/H \leq 0.10$, the friction factor provides an increase. The $g/H = 0.15$, 0.20, 0.25, 0.30, and 0.35 cases nearly perform values of friction factor.

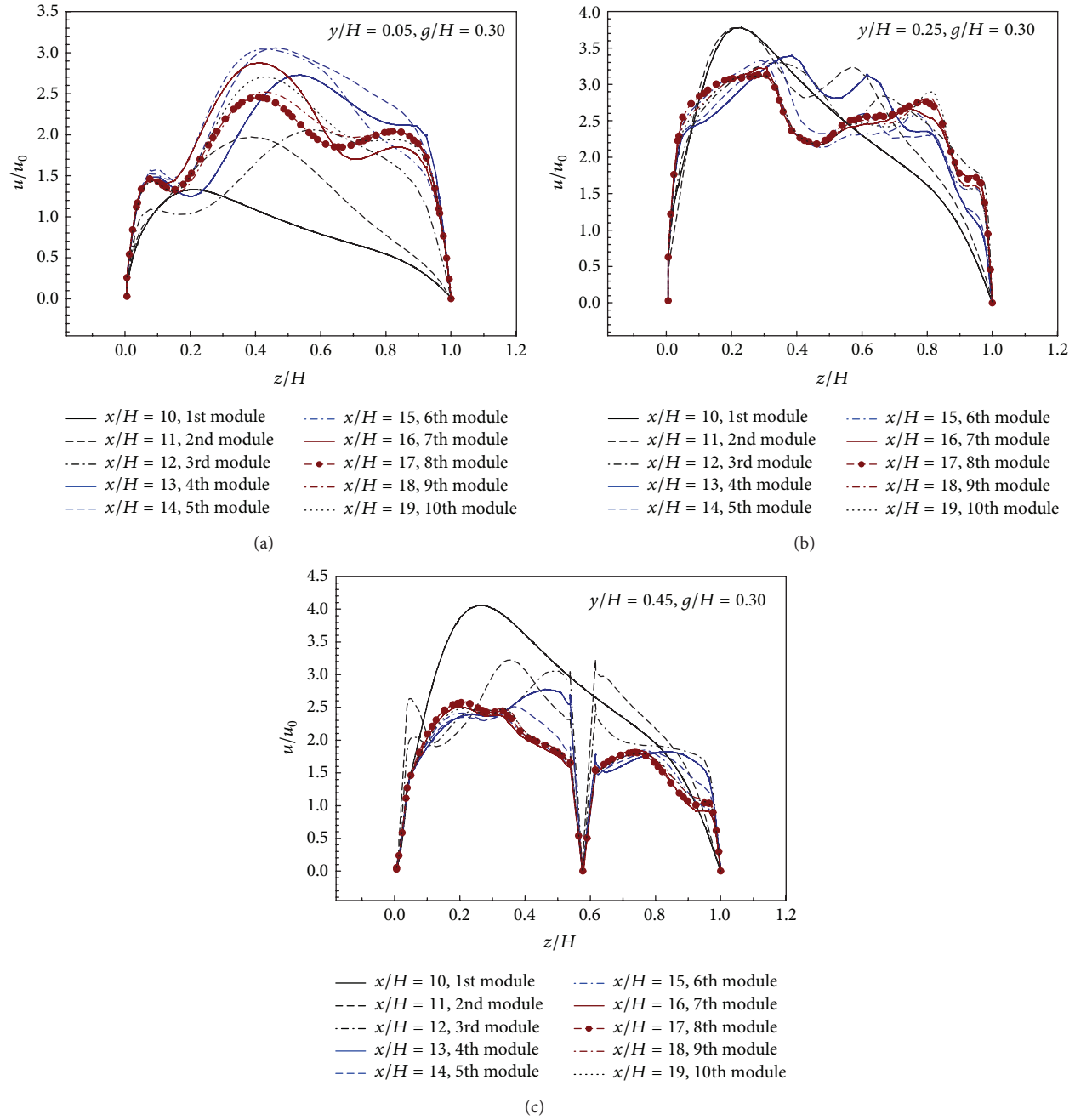

FIGURE 18: The variations of u/u_0 with z/H at various $y/H = 0.05$, 0.25, and 0.45 for $g/H = 0.30$ and Re = 800.

(ii) The difference of g/H leads to the variation of the flow configurations. The decreasing continuous flow areas perform the rise up for the number of the small vortex flows.

(iii) The visualizations of flow structure in the form of streamlines in transverse planes can describe the flow pattern as two groups: developing flow and periodic flow. The developing flow profiles appear earlier in the tested section when the periodic flow profiles, similar to flow structures, are found after the flow passes around the 6th module.

(iv) The numerical results in terms of variations of u/u_0 with positions can be concluded in the velocity profiles as two sections: periodic flow profile and fully developed flow profile. The periodic flow profiles mean that the flow structures have similar configurations but are different from the velocity values while the fully developed periodic flow profiles, the configurations and values of velocity are equal.

(v) In the range studied, the periodic flow profiles appear around the 2nd module and the fully developed periodic flow profiles show around the 6th–9th modules.

Table 2: The flow area descriptions.

Case	Upper flow area	Lower flow area	Middle flow area
$g/H = 0$	0	0	0.70
$g/H = 0.05$	0.05	0.05	0.60
$g/H = 0.10$	0.10	0.10	0.50
$g/H = 0.15$	0.15	0.15	0.40
$g/H = 0.20$	0.20	0.20	0.30
$g/H = 0.25$	0.25	0.25	0.20
$g/H = 0.30$	0.30	0.30	0.10
$g/H = 0.35$	0.35	0.35	0

Close to the RVG regimes and decreasing continuous flow area, the flow profiles perform the speed-up of fully developed periodic flow profiles.

Conflict of Interests

The author declares that there is no conflict of interests regarding the publication of this paper.

Acknowledgments

This research was funded by King Mongkut's Institute of Technology Ladkrabang, Bangkok, Thailand. The author would like to thank Associate Professor Dr. Pongjet Promvonge and Mr. Jaray Wongpueng for suggestions.

References

[1] S. Sripattanapipat and P. Promvonge, "Numerical analysis of laminar heat transfer in a channel with diamond-shaped baffles," *International Communications in Heat and Mass Transfer*, vol. 36, no. 1, pp. 32–38, 2009.

[2] P. Promvonge, S. Sripattanapipat, S. Tamna, S. Kwankaomeng, and C. Thianpong, "Numerical investigation of laminar heat transfer in a square channel with 45° inclined baffles," *International Communications in Heat and Mass Transfer*, vol. 37, no. 2, pp. 170–177, 2010.

[3] P. Promvonge, W. Jedsadaratanachai, and S. Kwankaomeng, "Numerical study of laminar flow and heat transfer in square channel with 30° inline angled baffle turbulators," *Applied Thermal Engineering*, vol. 30, no. 11-12, pp. 1292–1303, 2010.

[4] P. Promvonge, S. Sripattanapipat, and S. Kwankaomeng, "Laminar periodic flow and heat transfer in square channel with 45◦ inline baffles on two opposite walls," *International Journal of Thermal Sciences*, vol. 49, no. 6, pp. 963–975, 2010.

[5] W. Jedsadaratanachai, S. Suwannapan, and P. Promvonge, "Numerical study of laminar heat transfer in baffled square channel with various pitches," *Energy Procedia*, vol. 9, pp. 630–642, 2011.

[6] P. Promvonge, W. Jedsadaratanachai, S. Kwankaomeng, and C. Thianpong, "3D simulation of laminar flow and heat transfer in V-baffled square channel," *International Communications in Heat and Mass Transfer*, vol. 39, no. 1, pp. 85–93, 2012.

[7] W. Jedsadaratanachai, N. Jayranaiwachira, and P. Promvonge, "Computational investigation on fully developed periodic laminar flow structure in baffled circular tube with various BR," *Mathematical Problems in Engineering*, vol. 2014, Article ID 735905, 9 pages, 2014.

[8] H. K. Versteeg and W. Malalasekera, *An Introduction to Computation Fluid Dynamics*, Pearson Education, 2nd edition, 2007.

[9] S. Kwankaomeng and P. Promvonge, "Numerical prediction on laminar heat transfer in square duct with 30° angled baffle on one wall," *International Communications in Heat and Mass Transfer*, vol. 37, no. 7, pp. 857–866, 2010.

[10] P. Promvonge and S. Kwankaomeng, "Periodic laminar flow and heat transfer in a channel with 45° staggered V-baffles," *International Communications in Heat and Mass Transfer*, vol. 37, no. 7, pp. 841–849, 2010.

[11] A. Boonloi, "Effect of flow attack angle of v-ribs vortex generators in a square duct on flow structure, heat transfer, and performance improvement," *Modelling and Simulation in Engineering*, vol. 2014, Article ID 985612, 11 pages, 2014.

[12] A. Boonloi and W. Jedsadaratanachai, "3D Numerical study on laminar forced convection in V-baffled square channel," *The American Journal of Applied Sciences*, vol. 10, pp. 1287–1297, 2013.

[13] W. Jedsadaratanachai and A. Boonloi, "Energy performance improvement, flow behavior and heat transfer investigation in a circular tube with V-downstream discrete baffles," *Journal of Mathematics and Statistics*, vol. 9, pp. 339–348, 2013.

[14] W. Jedsadaratanachai and A. Boonloi, "Effect of twisted ratio on flow structure, heat transfer and thermal improvement in a circular tube with single twisted tape," *Journal of Mathematics and Statistics*, vol. 10, pp. 80–91, 2014.